Propagation of postsynaptic currents and potentials via gap junctions in GABAergic networks of the rat hippocampus

Veronika Zsiros[1], Ildiko Aradi[1] and Gianmaria Maccaferri[1,2]

[1]*Department of Physiology, Feinberg School of Medicine and* [2]*Institute for Neuroscience, Northwestern University, Chicago, IL 60611, USA*

The integration of synaptic signalling in the mammalian hippocampus underlies higher cognitive functions such as learning and memory. We have studied the gap junction-mediated cell-to-cell and network propagation of $GABA_A$ receptor-mediated events in stratum lacunosum moleculare interneurons of the rat hippocampus. Propagated events were identified both in voltage- and current-clamp configurations. After blockade of ionotropic excitatory synaptic transmission, voltage-clamp recordings with chloride-loaded electrodes (predicted $GABA_A$ receptor reversal potential: 0 mV) at −15 mV revealed the unexpected presence of spontaneous events of opposite polarities. Inward events were larger and kinetically faster when compared to outward currents. Both types of events were blocked by gabazine, but only outward currents were significantly affected by the gap junction blocker carbenoxolone, indicating that outward events originated in electrically coupled neurons. These results were in agreement with computational modelling showing that propagated events were modulated in size and shape by their relative distance to the gap junction site. Paired recordings from electrically coupled interneurons performed with high- and low-chloride pipettes (predicted $GABA_A$ receptor reversal potentials: 0 mV and −80 mV, respectively) directly demonstrated that depolarizing postsynaptic events could propagate to the cell recorded with the low-chloride solution. Cell-to-cell propagation was abolished by carbenoxolone, and was not observed in uncoupled pairs. Application of 4-aminopyridine on slices resulted in spontaneous network activation of interneurons, which was driven by excitatory $GABA_A$ receptor-mediated input. Population activity was greatly depressed by carbenoxolone, suggesting that propagation of depolarizing synaptic GABAergic potentials may be a critical determinant of interneuronal synchronous bursting in the hippocampus.

(Received 25 October 2006; accepted after revision 10 November 2006; first published online 16 November 2006)
Corresponding author G. Maccaferri: Department of Physiology, Northwestern University, Feinberg Medical School, 303 E Chicago Ave, Tarry Blg Rm 5-707 M211, Chicago, IL 60611, USA. Email: g-maccaferri@northwestern.edu

The integration of chemical and electrical signalling (Bennett & Zukin, 2004; Connors & Long, 2004) in the mammalian brain is believed to play an essential role for the regulation of neuronal networks. Hippocampal GABAergic interneurons have been shown to be interconnected via both chemical synapses and gap junctions (Venance *et al.* 2000; Bartos *et al.* 2001; 2002; Meyer *et al.* 2002; Zhang *et al.* 2004; Price *et al.* 2005; Zsiros & Maccaferri, 2005), similarly to what was described in neocortical circuits (reviewed by Hestrin & Galarreta, 2005). Electrical coupling in these networks is thought to be predominantly dependent on the expression of connexion 36 (Cx36, Venance *et al.* 2000; Deans *et al.* 2001; Hormuzdi *et al.* 2001), assembled to form functional gap junction channels (Srinivas *et al.* 1999; Teubner *et al.* 2000). Therefore, hippocampal interneurons are an ideal cellular population for the study of the gap junction-mediated propagation of chemical input and of its impact during synchronized network activity. Although previous work at both invertebrate and non-cortical synapses has suggested or even directly shown that postsynaptic potentials may backpropagate through gap junctions (for example, Martin & Pilar, 1963; Decima, 1969; Zipser & Bennett, 1976; Marder & Eisen, 1984; Slesinger & Bell, 1985; Pereda *et al.* 1995; for a review of electrical coupling in the mammalian brain see Connors & Long, 2004; for a general review see Bennett, 1977), most of those studies were focused on antidromic transmission from postsynaptic sites to presynaptic terminals. In contrast, neurons of mammalian GABAergic cortical networks are believed to be coupled by gap

V. Zsiros and I. Aradi contributed equally to this work.

DOI: 10.1113/jphysiol.2006.123463

junctions located at somatic or dendritic sites (Kosaka & Hama, 1985; Fukuda & Kosaka, 2000; Szabadics *et al.* 2001; Simon *et al.* 2005; Fukuda *et al.* 2006). Furthermore, no paired recording study has ever addressed quantitatively the propagation of unambiguously identified synaptic signals in mammalian cortical interneurons.

Interneuronal networks in the stratum lacunosum moleculare of the hippocampus are especially interesting because they have been shown to react to exogenous GABA application with an all-or-none synchronized response (Perkins, 2002), suggesting that electrical coupling may be especially important in the recruitment of the elements of the assembly. Intriguingly, stratum lacunosum moleculare interneurons appear to have a diffuse electrical connectivity. For example, the percentage of double recordings showing electrical coupling in slices has been reported to range between 33% (Zsiros & Maccaferri, 2005) and 85% (Price *et al.* 2005).

Here, we have designed experiments with three main purposes: (i) to provide evidence for the propagation of unambiguously identified chemical input across coupled elements of the network; (ii) to quantify the degree of propagation in pairs of neurons; and (iii) to assess the role of electrical coupling during a dynamic model of network activity, which is driven by $GABA_A$ receptor-mediated excitatory input (Perrault & Avoli, 1989, 1992; Lamsa & Kaila, 1997; Perkins, 2002).

We propose that the interplay between chemical input and electrical synapses enhances divergence within the network and acts as a recurrent circuit, which is an important determinant of population activity in the hippocampus.

Methods

Slice preparation

Slices were prepared from young rats (P12–P23). Rats were first deeply anaesthetized using isoflurane (∼0.5–1 ml and inhalation to effect) in an induction chamber, in compliance with the guidelines provided by the IACUC of Northwestern University and the National Institutes of Health (NIH). The level of anaesthesia was assessed by monitoring the pedal withdrawal reflex and by pinching the tail and ears. Following deep anaesthesia, rats were quickly decapitated and the brain removed from the skull in a small container filled with chilled solution of the following composition (mM): 234 sucrose, 28 $NaHCO_3$, 2.5 KCl, 1.25 NaH_2PO_4, 0.5 CaCl2, 7 $MgSO_4$, 7 glucose, 1 ascorbic acid, 3 pyruvic acid saturated with 95% O_2, 5% CO_2 at pH 7.4. Both hemispheres of the brain were glued onto the stage of a vibrating microtome (Leica, VT 1000S), submerged with chilled artificial cerebrospinal fluid (ACSF), and sections of 300–400 μm were cut and stored in an incubation chamber at 34–35°C for at least 30 min, then stored at room temperature until use.

Whole-cell recordings

Conventional patch-clamp recordings were performed. Slices were superfused with preheated ACSF maintained at a constant temperature (32–35°C). ACSF was of the following composition: (mM) 130 NaCl, 24 $NaHCO_3$, 3.5 KCl, 1.25 NaH_2PO_4, 2 $CaCl_2$, 1 $MgSO_4$, 10 glucose saturated with 95% O_2, 5% CO_2 at pH = 7.4. In order to increase the frequency of spontaneous events, in nine current-clamp experiments with connected pairs, external potassium was raised up to to 7.5 mM. Cells were observed and selected for recording by means of 40× IR immersion DIC objective applied to a direct microscope (Olympus, Japan) equipped with an infrared camera system (DAGE-MTI, Michigan City, IN, USA). Interneurons were selected in the CA1 stratum lacunosum moleculare, according to the same criteria as in Zsiros & Maccaferri (2005). Pipettes were pulled from borosilicate thin glass capillaries (MTW150F-3, WPI) and filled with the appropriate filtered intracellular solution to a 1.5–5 MΩ final resistance, as detailed below. Recordings were carried out using a Multiclamp 700 amplifier (Molecular Devices, Sunnyvale, CA, USA). Data were filtered at 3 KHz and digitized at 10–20 kHz using a Digidata A/D board and the Clampex 9 program suite (Molecular Devices). Series resistances were constantly monitored by injecting a- 5/10 mV step in voltage-clamp or a −50/100 pA pulse in current-clamp configuration. Series resistances were not compensated in voltage-clamp configuration, whereas they were balanced via a bridge circuit in current-clamp mode. Liquid junction potential (V_{jp}; by convention in the direction of the batch relative to the pipette: $V_{jp} = V_{bath} - V_{pipette}$) was experimentally estimated (Neher, 1992; Figl *et al.* 2004) and subtracted offline, so that for voltage-clamp experiments $V_{holding} = V_{command} - V_{jp}$ and for current-clamp experiments $V_{membrane} = V_{recorded} - V_{jp}$.

Low-chloride solution for current-clamp recordings . The composition of this solution was (mM): 125 K-methylsulphate, 4 ATP-Mg_2, 4 NaCl, 0.3 GTP, 16 $KHCO_3$ equilibrated with 95% O_2, 5% CO_2 to a pH 7.3. Estimated reversal potential for $GABA_A$ (as detailed in Aradi & Maccaferri, 2004) was −80 mV. V_{jp} was ∼+10 mV.

High-chloride solution for current-clamp recordings. The compostition of this solution was (mM): 125 KCl, 4 ATP-Mg_2, 10 NaCl, 0.3 GTP, 16 $KHCO_3$ equilibrated with 95% O_2, 5% CO_2 to a pH 7.3. Estimated reversal potential for $GABA_A$ was −2 mV. For the purpose of simplicity

and comparison with voltage-clamp recordings reversal potential for $GABA_A$ is considered to be ∼0 mV in the Result section. V_{jp} was ∼+5 mV.

Low-chloride solution for voltage-clamp recordings. The composition of this solution was (mM): 125 K-methylsulphate, 4 ATP-Mg_2, 4 NaCl, 0.3 GTP, 16 $KHCO_3$, 5 *N*-2(2,6-dimethylphenylcarbamoylmethyl) triethylammonium chloride (QX-314-Cl) and 0.2% biocytin equilibrated with 95% O_2, 5% CO_2 to a pH 7.3. Estimated reversal potential for $GABA_A$ was −66 mV. QX-314 was included in the intracellular solution at high concentration in order to block voltage-dependent conductances and $GABA_B$ receptor-operated potassium currents. V_{jp} was ∼+10 mV.

High-chloride solution for voltage-clamp recordings. The composition of this solution was (mM): 125 KCl (or CsCl), 4 ATP-Mg_2, 10 NaCl, 0.3 GTP, 16 $KHCO_3$, 5 *N*-2(2,6-dimethylphenylcarbamoylmethyl) triethylammonium chloride (QX-314-Cl) and 0.2% biocytin equilibrated with 95% O_2, 5% CO_2 to a pH 7.3. Estimated reversal potential for $GABA_A$ was 0 mV. QX-314 was included in the intracellular solution at high concentration in order to block voltage-dependent conductances and $GABA_B$ receptor-operated potassium currents. V_{jp} was ∼+5 mV.

Holding potential for voltage-clamp recordings. The holding potential for voltage-clamp experiments was set to −15 mV in the experiments shown in Figs 1, 4, and 6*D*.

In the case of the voltage-clamp experiments shown in Figs 5*A* and 6*A–C*, the holding potential was set at more hyperpolarized potentials (−30 mV) because we had the impression that this improved the stability required for pharmacological tests (25 min of drug application). In these latter cases, cells in which outward currents were not observed were not included in this study.

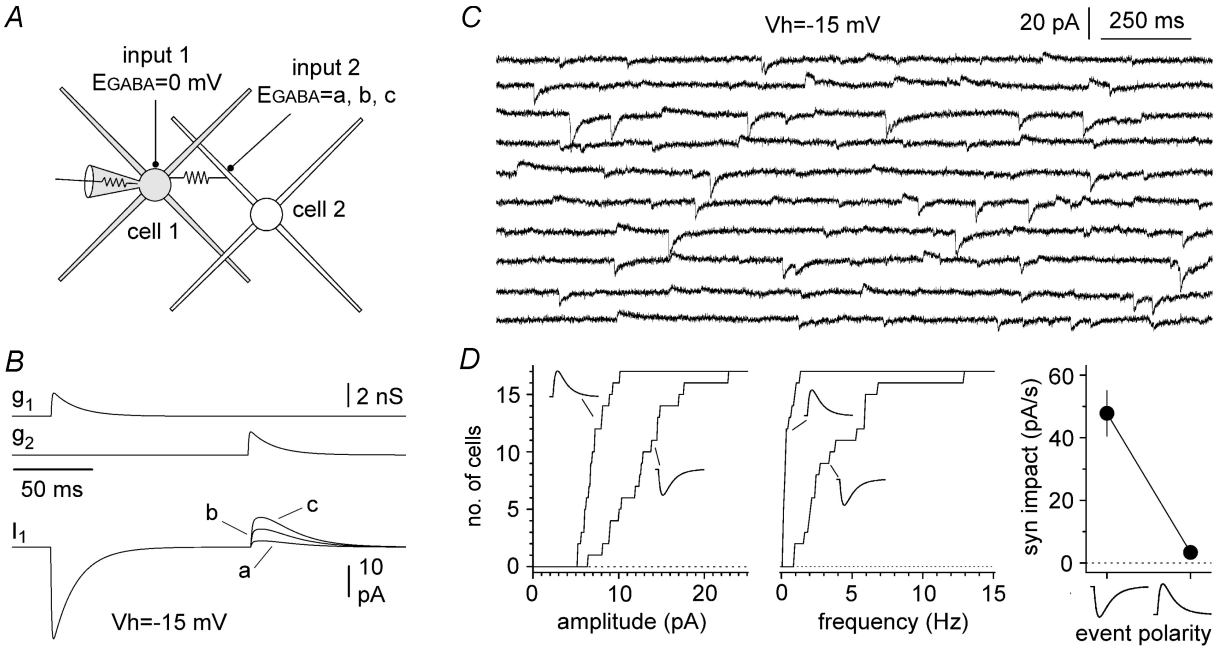

Figure 1. Propagation of GABAergic postsynaptic currents via gap junctions: computational and experimental approach

A, computational model of two small multipolar interneurons (cell 1, and cell 2) connected by a gap junction (2 nS), and receiving independent GABAergic input (input 1, and input 2). Four dendrites (100 μm length, thickness proximal → distal 1.5 → 0.2 μm, 20 compartments) and a soma (diameter 15 μm, two compartments) were used (for more details see Methods). *B*, sequential activation of the synaptic conductances gated by input 1 (g_1) and input 2 (g_2) in the model cells. Simulated voltage-clamp conditions in model cell 1 ($V_{holding} = -15$ mV), generated currents with opposite polarities (input 1 → inward and input 2 → outward). E_{GABA} was set to 0 mV for cell 1, whereas three different E_{GABA} values were tested for cell 2 ($a = -50$ mV, $b = -60$ mV, $c = -70$ mV). *C*, experimental traces of spontaneous events recorded in an interneuron at a holding potential of −15 mV. Notice that both inward and outward postsynaptic currents can be observed. Because outward events occurred much more rarely than inward currents, sweeps were selected non-contiguously. *D*, properties of inward and outward events recorded. Cumulative distribution plots of the amplitude and frequency of recorded events are shown in the left and middle panel, respectively. Distributions for inward and outward events are indicated by the appropriate polarity symbol. Right panel: comparisons of the synaptic impact (syn impact) for inward and outward events: the impact of outward currents is ∼7% of the one calculated for inward events at −15 mV. Excitatory synaptic transmission and slow inhibition were blocked pharmacologically (see Methods for details).

Non-invasive cell-attached measurement of membrane potential

In order to avoid the potential disruption of intracellular gradients caused by whole-cell recording configuration, non-invasive measurement of membrane potential was performed in cell-attached mode, similarly to what is described in Morikawa *et al.* (2003). Briefly, low-resistance electrodes (∼1.5 MΩ) when filled with ACSF were used in cell-attached configuration. After verification of the formation of a tight seal (>2 GΩ) in voltage-clamp configuration, the amplifier was switched to $I = 0$ mode, and the membrane potential was recorded. Cell-attached configuration was then monitored by switching back to voltage-clamp mode and by delivering voltage steps (250 ms duration, −10 mV amplitude) from a holding potential of −60 mV. Pressure-induced or spontaneous breakthrough of this configuration was also easily detected in current-clamp mode as an abrupt depolarization of the membrane potential.

Evaluation of electrical coupling and junctional conductance in paired current-clamp experiments

We tested for the presence of gap junctions between pairs by repetitively injecting a 500 ms current step of −100 pA. Cells were considered coupled if they had a DC coefficient coupling (ratio of the voltage deflection in the non-injected cell to the voltage deflection in the injected cell measured during the last 50 ms of the stimulus) value higher than 0.005, and the shape of the electrotonic response was recognizable in the recording from the non-injected cell. The synaptic coupling coefficient was calculated as the ratio of the peak of the postsynaptic potential recorded in the cell with the low-chloride solution to the peak of the synchronous event measured in the chloride-loaded neuron. The effective junctional conductance (G_j) was calculated according to the equation

$$G_j = \frac{1}{[(R_{in2}/CC) - R_{in2}]}$$

where R_{in2} is the input resistance of the non-injected neuron and CC is the DC coefficient coupling. This calculation is based on the assumption of two isopotential neurons connected by a single electrical junction (Bennett, 1977).

Drug preparation and application in slices

All the following drugs were from Tocris Biosciences. SR-95531 (gabazine) was used at 12.5 μM. The powder was dissolved in water as a stock solution at 25 mM, aliquoted in 100 μl vials, and frozen at −20°C. D–AP5 was dissolved in water, stocked frozen in 100 μl aliquots at 50 mM and used at 50 μM. Stock solutions of NBQX were dissolved in DMSO at 100 mM, aliquoted in 40 μl vials and frozen at −20C. The final concentration used was 20 μM. CGP55845 was dissolved in DMSO in stock solutions at 100 mM, then aliquoted and used at a final concentration of 1–5 μM. Carbenoxolone was obtained from Sigma as a disodium salt, and was dissolved directly into the recording solution to a final concentration of either 100 or 500 μM. 4-Aminopyridine was from Sigma and was also dissolved directly into the recording solution to its final concentration of 50–100 μM.

Analysis of spontaneous events in single cell recordings

Spontaneous currents recorded from single neurons held at depolarized potentials were analysed using the Clampfit 9.0 (Molecular Devices), Origin Pro7.0 (OriginLab, Northampton, MA, USA), and Microsoft Excel suites of programs. Events were first collected using the template-based analysis feature of Clampfit, and then reviewed by visual inspection. However, under our experimental conditions at depolarized potentials, a significant fraction of the events were below detection levels, leading to potential ambiguities in the interpretation of measured amplitude and frequency (Stell & Mody, 2002). Therefore, we used the 'largest-amplitude count matching' method developed by Stell & Mody (2002) to build the I–V relationship in Fig. 2. The number of events matched for inward currents was 146 ± 40 ($n = 7$) and 10 ± 1 ($n = 7$) for outward events. Largest-amplitude count matching could not be used in the pharmacological analysis of Figs 5 and 6 because of the reduced number of observations due to the effect of the drugs themselves. Therefore, we combined amplitude and frequency in a single index as 'synaptic impact' (event amplitude multiplied by its frequency, see Galarreta & Hestrin, 1998), which is related to the synaptic effect on average membrane potential, provided that the kinetics of events are unchanged (Tsodyks & Markram, 1997; Abbott *et al.* 1997).

Analysis of synchronous synaptic events in paired recording

Analysis of synchronous postsynaptic potentials was performed by using the WinEDR and WinWCP software package (courtesy of Dr J. Dempster, University of Strathclyde, UK). The rising phase of the depolarizing events in the cell recorded with high-chloride solution was used to trigger acquisition in both channels. Events were then inspected visually; obviously distorted records were rejected and not used for the analysis.

Analysis of network-driven events in slices exposed to 4-aminopyridine

Spontaneous network currents recorded from single neurons were analysed using the Clampfit 9.0, OriginPro7.0, and Microsoft Excel suites of programs. Events were first collected using the threshold-based analysis feature of Clampfit, reviewed by visual inspection, and aligned by their peaks. *I–V* plots shown in Fig. 9 were built from spontaneous events collected in ∼5 min epochs (for example, 8 ± 2 events at holding potential (V_h) = –65 mV in Fig. 9*A*, $n = 5$ cells, and 7 ± 1 events at $V_h = -70$ mV for Fig. 9*C*, $n = 5$ cells). Analysis of the time course of the effect of carbenoxolone (and long recording) presented in Fig. 11 was performed first by averaging the amplitudes of spontaneous events within the same neuron in 1 min bins and then by averaging each bin across different cells.

Analysis of spike afterhyperoplarizations

Trains of spikes were evoked by current steps injected through the whole-cell electrode (1 s duration, 100–350 pA amplitude). Spikes collected from 20 sweeps were aligned and averaged in control conditions and after application of gabazine (12.5 μM). After-hyperpolarizations were measured from action potential threshold (defined as the membrane potential at which dV/dt exceeds 10 V s^{-1} (Fricker *et al.* 1999)) to the negative peak of the hyperpolarization. Cell membrane potential was maintained close to the resting potential of the cells between −65 and −70 mV.

Statistical methods

Statistical analysis was performed using the following software packages: Clampfit 9.0, Excel, Origin, Prism (Graphpad, San Diego, CA, USA), Win EDR, and Win WCP. Non-parametric tests (Wilcoxon signed test, abbreviated as W, Mann–Whitney test, abbreviated as M–W, and Kruskal–Wallis test, abbreviated as K–W) were used, as appropriate. Data are shown as mean ± S.E.M.

Computational methods

We performed simulations using the NEURON 5.4 software (Hines & Carnevale, 1997) running on Linux. The model interneurons had a soma and four dendrites to resemble the morphology of multipolar interneurons located in the stratum lacunosum moleculare. We included voltage-activated channels Na^+, delayed rectifier K^+, and A-type K^+ channels (the kinetics of the channels

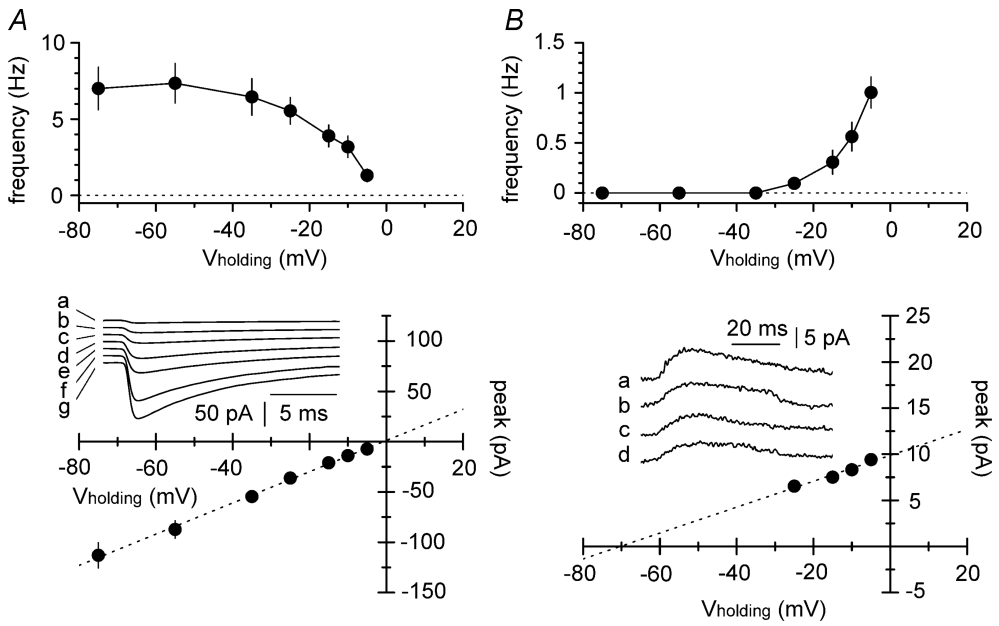

Figure 2. Frequency–voltage and current–voltage relationships for inward and outward events
A, top panel: the ability to detect inward currents is reduced by depolarized holding potentials. Notice the apparent voltage-dependency of the frequency of the detected events. Bottom panel: the current–voltage relationship built according to the 'largest-amplitude count matching method' (see Methods for details). Notice that the extrapolated reversal potential is close to the predicted value of 0 mV. Experimental data were fitted by linear regression (dotted line, $y = 1.551x + 1.114$, $r^2 = 0.999$, $P < 0.05$). Experimental traces are shown at different holding potentials ($a = -5$ mV, $b = -10$ mV, $c = -15$ mV, $d = -25$ mV, $e = -35$ mV, $f = -55$ mV, and $g = -75$ mV). *B*, top and bottom panels: similar analysis of frequency and amplitude voltage-dependency performed for outward currents. The estimated reversal potential was −70 mV (regression line was $y = 0.1405x + 9.88$, $r^2 = 0.999$, $P < 0.05$). Insets show currents recorded at various holding potentials ($a = -5$ mV, $b = -10$ mV, $c = -15$ mV, $d = -25$ mV).

were taken from Aradi & Holmes, 1999; and Yamada *et al.* 1989). The morphological and biophysical parameters were as follows: (i) soma: diameter = 15 μm, number of compartments = 2, maximal conductance values for sodium conductance (g_{Na}) = 150 mS cm^{-2}; delayed rectifier potassium conductance ($g_{K\text{-}DR}$) = 40 mS cm^{-2} and A-type potassium channel conductance ($g_{K\text{-}A}$) = 2.55 mS cm^{-2}; (ii) dendrites: length = 100 μm, diameter: proximal= 1.5 μm, distal = 0.2 μm, number of compartments = 20, maximal conductance values for g_{Na} = 13 mS cm^{-2}, $g_{K\text{-}DR}$ = 4 mS cm^{-2}. Resting membrane potential was set at −65 mV, and membrane specific capacitance was 3 μF cm^{-2}. We used a relatively high value of specific capacitance to compensate for the oversimplified anatomical structure of the model, which includes only four dendrites and is likely to underestimate the global membrane capacitance of the neuron. As shown in Supplementary Fig. 1, the selected value of specific capacitance produces DC and spike coefficient coupling that are similar to those reported experimentally in the literature (compare with Zsiros & Maccaferri, 2005 and Price *et al.* 2005). Furthermore, our approach should be considered conservative because a more standard value of specific capacitance such as 1 μF cm^{-2} would enhance coupling in the model (see Supplementary Fig. 1). Voltage-dependent conductances were set to 0 mS cm^{-2} in the model cell under simulated voltage-clamp conditions to mimic the effect of QX-314. The input resistance for these model neurons was 250 MΩ (Price *et al.* 2005). Specific and axial resistance were set to 4347.8 Ω cm^2 and 210 Ω cm, respectively. Two interneurons were coupled by a junctional conductance (G_j, 0.5 or 2 nS), which connected the soma of cell 1 to the mid-dendrite of cell 2. Gap junction coupling was modelled by a current (I_{Gj}) proportional to the potential difference between the two cells at the gap junction site, i.e. $I_{Gj1} = G_j(V_2 - V_1)$ in the first cell, where G_j is the junctional conductance, and $I_{Gj2} = -I_{Gj1}$ in the second cell. The kinetics of the postsynaptic conductance were described by the following equation:

$$g_{GABA} = G_{peak}(e^{\frac{-t}{\tau_{decay}}} - e^{\frac{-t}{\tau_{rise}}})$$

with G_{peak} = 2 nS, rise time constant (τ_{rise}) = 0.5 ms and decay time constant (τ_{decay}) = 15 ms. A time step of 0.01 ms was used in the simulations.

Results

Voltage-clamp analysis of event propagation: computational modelling and *in vitro* recordings

In order to explore potential experimental scenarios, we built a computational model of a small network consisting of two multipolar interneurons (cell 1 and cell 2, Fig. 1*A*). The two model cells were connected by a gap junction, and both received exclusively $GABA_A$ receptor-mediated synaptic input. The basic characteristics of the model neurons were mostly tailored on the available data in the literature for neurogliaform cells (Price *et al.* 2005; Zsiros & Maccaferri, 2005). Provided that the reversal potential for GABAergic input (E_{GABA}) in the two cells could be set to different values, then voltage clamping one cell of the pair (cell 1) at an intermediate holding potential (set between the two different E_{GABA} values) should distinguish direct synaptic input from gap junction-propagated events because of their different polarities. Figure 1*B* shows the results of a set of simulations with a holding potential of −15 mV. E_{GABA} was set to 0 mV in cell 1, whereas it was set, alternatively, to −50 mV, −60 mV, and −70 mV in cell 2. Sequential activation of identical GABAergic conductances in the two different model cells resulted in postsynaptic currents in cell 1, but with opposite polarities and different amplitudes.

We directly tested this prediction by recording spontaneous $GABA_A$ receptor-mediated synaptic activity from stratum lacunosum moleculare interneurons in hippocampal slices, using a medium containing blockers of glutamatergic and $GABA_B$ receptor-mediated synaptic transmission (Fig. 1*C*). We took advantage of the whole-cell recording configuration, and used a chloride-loaded pipette to manipulate E_{GABA} in the recorded neuron (calculated value: 0 mV, see Methods for details). We reasoned that chloride loading would remain mostly restricted to the cell under voltage clamp, and should not spread significantly to other neurons that are electrically coupled to it. This assumption relies on work showing that: (i) various connexin channels or hemichannels have low chloride relative permeability (Beblo & Veenstra, 1997; Eskandari *et al.* 2002); (ii) Cx36 channels have undetermined anionic selectivity; and (iii) the lowest conductance reported within the connexin family (Srinivas *et al.* 1999); and, lastly (iv) that interneurons possess chloride clearance mechanisms, for example, via the KCC2 cotransporter (Gulyas *et al.* 2001). Therefore, in our experimental conditions, different E_{GABA} values should exist in the recorded cell compared to the unperturbed interneurons of the slice.

The results from 17 recordings confirmed the presence of both inward and outward spontaneous currents (Fig. 1*D*). When compared to inward currents, outward events were smaller (7.1 ± 0.3 pA *versus* 12.8 ± 1.0 pA, $n = 17$, $P < 0.05$, W-test) and occurred much less frequently (0.4 ± 0.1 Hz *versus* 4.0 ± 0.7 Hz, $n = 17$, $P < 0.05$, W-test). We further quantified these differences by calculating the synaptic impact (event amplitude multiplied by its frequency) for the different polarities. At a holding potential of −15 mV, the synaptic impact of the outward events was 3.4 ± 0.8 pA s^{-1}, compared to 47.8 ± 7.3 pA s^{-1} for inward currents

($n = 17, P < 0.05$, W-test). Thus, our experimental results were consistent with the prediction that voltage-clamp recording from a single neuron can reveal synaptic activity spreading from other elements of the network, in addition to direct chemical input.

Next, in order to assess the voltage dependency of inward and outward events, we recorded pharmacologically isolated $GABA_A$ receptor-mediated spontaneous activity at different membrane potentials. The frequencies of both inward and outward events were highly voltage dependent in the range tested (Fig. 2*A* and *B*, $P < 0.05$, $n = 7$ cells, K–W-test). This indicated that a significant proportion of the events fell below threshold detection, and that variations of the driving force at different holding potentials had a relevant impact on the fraction of detectable events (Stell & Mody, 2002). The extrapolated reversal potential of inward currents was −1 mV (Fig. 2*A*), which was very close to the predicted value of 0 mV. In addition, as expected for direct GABAergic input, the amplitude of inward events was larger at more hyperpolarized membrane potentials. In contrast, outward currents had an estimated reversal potential of −70 mV, and displayed opposite voltage dependency, so that events grew larger at more depolarized holding potentials (Fig. 2*B*). These experiments suggest that inward currents are the result of direct neurotransmitter release onto the chloride-loaded cell, whereas outward currents reflect events originating from cells with different E_{GABA} values (Lamsa & Taira, 2003; Vida *et al.* 2006), but electrically coupled to the recorded neuron.

If outward currents were events propagated via gap junctions, then their kinetics would be expected to undergo some form of filtering. We used the same configuration introduced in Fig. 1*A* and examined the location dependency of the kinetics of the propagated events by varying the position of the chemical synapse along the dendrites. As shown in Fig. 3*A*–*C*, location had a strong effect both on amplitude and rise time kinetics. Decay kinetics were also affected, but to a lesser degree. Therefore, we next analysed the kinetic properties of experimentally recorded spontaneous inward and outward currents (Fig. 4*A*). As expected, we found that inward currents had much faster rise and decay time kinetics. The 20–80% rise time was 0.6 ± 0.0 ms for inward currents, compared to 8.1 ± 1.1 ms for outward events (Fig. 4*B*, $P < 0.05$, $n = 17$ W-test) and the 100–37% decay time was 15.1 ± 1.0 ms for inward events compared to 29.3 ± 2.4 ms for outward currents (Fig. 4*B*, $P < 0.05$, $n = 17$, W-test). The two types of events appeared separated in two distinct clusters, when plotted along their kinetic axis (Fig. 4*C*).

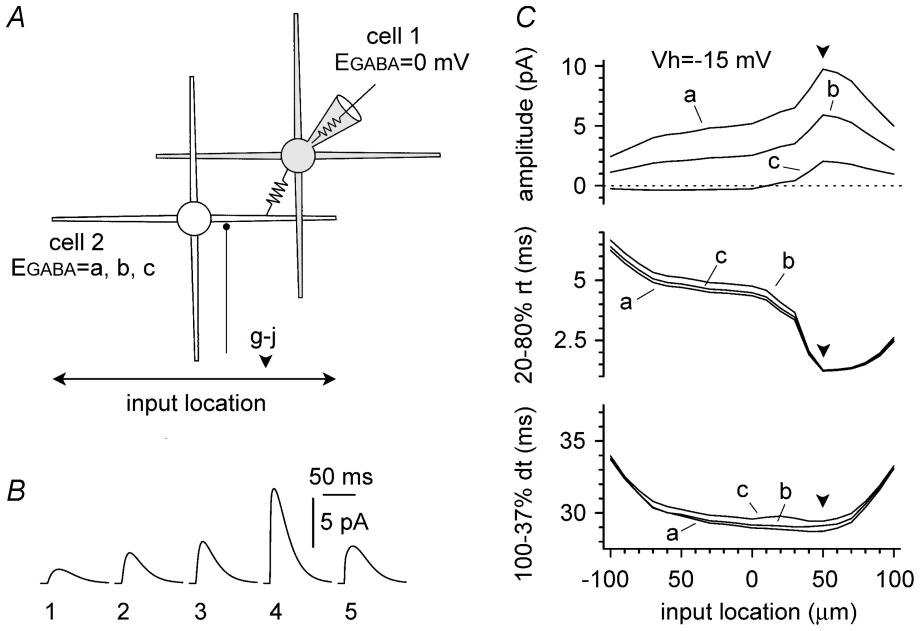

Figure 3. Simulations addressing the location dependency of the properties of the propagated events
Conditions were identical to Fig. 1*A*. A cartoon of the two-cell network: notice the fixed position of the gap junction (+50 μm, downward arrowhead) along the horizontal dendritic axis (from left to right: ±100 μm) and the variable position of the chemical input in cell 2 (double arrow). *B*, propagated events recorded on cell 1 plotted against the different locations in cell 2 (1 = −100 μm, 2 = −60 μm, 3 = soma, 4 = +50 μm, 5 = +100 μm). E_{GABA} was set to 0 mV in cell 1 and −60 mV in cell 2. *C*, summary plots showing the location dependency of the propagated input amplitudes (top panel), 20–80% rise times (middle panel), and 100–37% decay times (bottom panel). Plots were built from simulations with E_{GABA} in cell 1 set at 0 mV, and in cell 2 set at −70 mV, −60 mV, and −50 mV (indicated as *a*, *b*, and *c*, respectively).

Although the kinetics of averaged outward and inward currents were clearly different, spontaneous outward events with relatively fast time could be occasionally detected (see for example Fig. 6*A* and *D*). Possible explanations are: (i) that these events reflected release of neurotransmitter at sites closest to the gap junction, or that (ii) fast events propagated across intersomatic gap junctions, whereas slower events propagated across gap junctions located at more distal dendritic sites.

Pharmacological properties of spontaneous inward and outward GABAergic events

Next, we tested the pharmacological properties of outward currents recorded at depolarized potentials, and compared them to inward currents (Fig. 5*A*). Both inward and outward events were fully blocked by the $GABA_A$ receptor antagonist gabazine. Synaptic impact decreased from $28.4 \pm 9.0\,pA\,s^{-1}$ in control to 0.0 ± 0.0 pA in the presence of the drug for inward currents ($n = 5$, $P < 0.05$, W-test), and from $4.2 \pm 1.7\,pA\,s^{-1}$ to 0.0 ± 0.0 pA for outward currents ($n = 5$, $P < 0.05$, W-test). The sensitivity to gabazine suggests that it is unlikely that outward currents reflect the propagation of action potential afterhyperpolarization from coupled neurons. Nevertheless, we directly tested the gabazine sensitivity of current-evoked spike afterhyperpolarizations recorded from interneurons. Neither amplitude (16.1 ± 1.0 mV in control *versus* 15.8 ± 1.1 mV in the presence of the drug, $n = 10$, $P > 0.2$, W-test), nor the frequency (7.4 ± 1.8 Hz in control *versus*

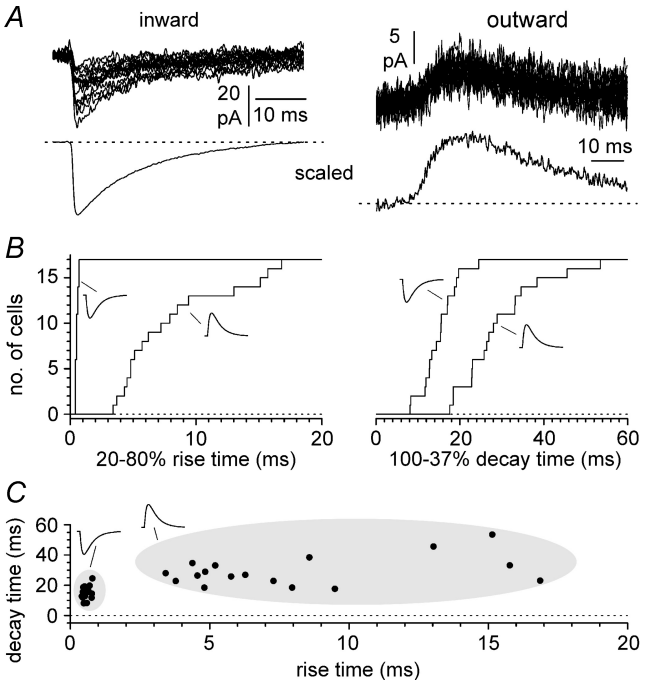

Figure 4. Kinetic analysis of inward and outward events recorded at depolarized potentials
A, sample traces of inward (left) and outward (right, $n = 25$ traces in both cases) recorded from the same cell at a holding potential of −15 mV. The lower insets show scaled averages to facilitate the comparison of the kinetics. *B*, cumulative distributions for 20–80% rise times and 100–37% decay times for inward and outward events (indicated by the appropriate polarity symbol). Notice the overall slower kinetics of outward events when compared to inward currents. *C*, summary plot of rise and decay times. Notice that inward and outward events appear well separated in distinct clusters (arbitrarily highlighted by the grey shading).

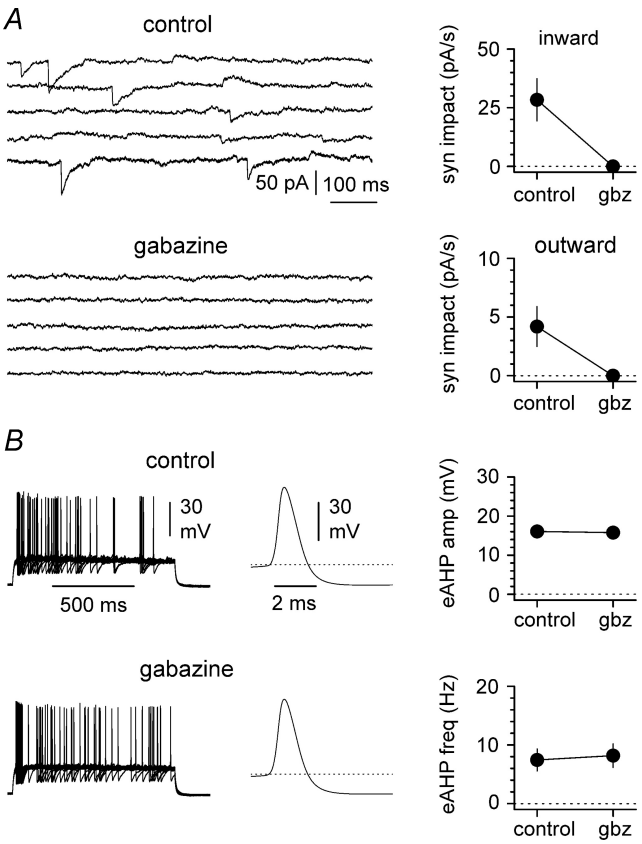

Figure 5. Spontaneous inward and outward currents are blocked by gabazine
A, regardless of the polarity, both events are sensitive to the $GABA_A$ receptor antagonist gabazine (gbz, 12.5 μM). Left: sweeps are shown in control conditions (upper inset) and in the presence of the drug (lower inset). Notice that gabazine abolishes all types of spontaneous activity. Sweeps were selected from non-contiguous epochs of the recording because of the lower frequency of outward events. Right: summary graph for $n = 5$ experiments, showing the effect of gabazine on the synaptic impact for inward (upper inset) and outward currents (lower inset). *B*, spike afterhyperpolarizations are not sensitive to gabazine. Left panel: superimposed trains of current-evoked action potentials ($n = 20$ sweeps) in control conditions (upper inset) and after the addition of the drug (lower inset). Middle panel: average of the mean action potential obtained from 10 interneurons in control conditions (upper inset) and after exposure to gabazine (lower inset). Right panel: summary plots for current-evoked spike afterhyperpolarization (eAHP) amplitude (upper plot) and frequency (lower plot) in the absence and the presence of gabazine (12.5 μM). Notice the lack of effect of the drug on either variable. Action potential threshold is indicated by the dotted line.

8.2 ± 2.0 Hz, $n = 10$, $P > 0.2$, W-test) of current-evoked spike afterhyperpolarization was affected by gabazine (Fig. 5*B*). If inward and outward events truly reflected GABAergic input originating from different electrically coupled cells, then gap junction blockers would be expected to predominantly affect the propagated events. Indeed, as shown in Fig. 6*A* and *B*, the gap junction uncoupler carbenoxolone (100 μM) had no significant effect on the synaptic impact of inward events (from 34.9 ± 12.0 pA s^{-1} in control to 34.8 ± 5.5 pA s^{-1} after 25 min in the presence of the drug ($n = 8$, $P > 0.2$, W-test), whereas outward currents were reduced from 3.3 = 8 ± 1.0 pA s^{-1} in control to 0.5 ± 0.2 pA s^{-1} after 25 min of carbenoxolone application ($n = 8$, $P < 0.05$, W-test). We also performed control experiments to exclude the possibility of time-dependent run-down (Fig. 6*C*). After the control period, 25 additional minutes in the absence of any drug did not change significantly the synaptic impact of either inward or outward currents (inward currents: from 69.9 ± 18.2 pA s^{-1} in control to 76.1 ± 21.9 pA s^{-1} after the 25 additional minutes ($n = 6$, $P > 0.2$, W-test), outward currents: from 1.9 ± 0.6 pA s^{-1} in control to 1.9 ± 0.4 pA s^{-1} after the 25 additional minutes ($n = 6$, $P > 0.2$, W-test)). Lastly, we studied the effect of carbenoxolone applied to the recorded neuron via the whole-cell pipette, in order to reduce

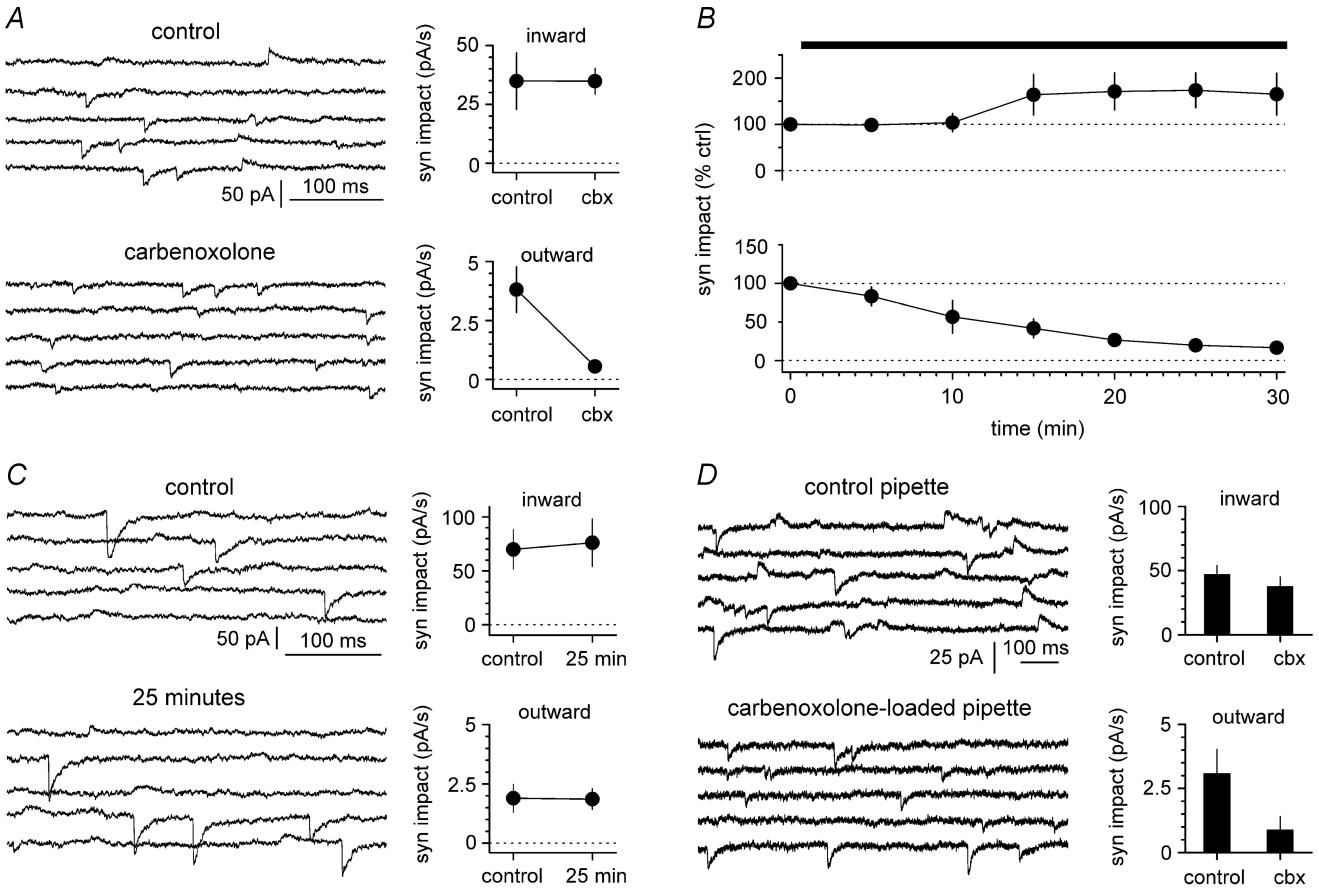

Figure 6. Carbenoxolone affects the synaptic impact of outward, but not inward currents
A, sweeps in control conditions and in the presence of the drug (100 μM, $n = 8$ experiments) are shown in the upper and lower left insets, respectively. Sweeps were selected from non-contiguous epochs of the recording because of the lower frequency of outward events. *B*, summary plot ($n = 8$ experiments until $t = 25$ mins, the last point and S.E.M. are from 7 cells) of the time course of the effect of the drug on the normalized synaptic impact for events of either polarity (inward currents: upper plot, outward currents: lower plot). Notice the polarity-dependent selectivity of the effect of the drug. The apparent potentiation of the synaptic impact of inward currents was not statistically significant. *C*, prolonged recordings without any drug application do not affect synaptic impact of spontaneous events. Left: non-contiguous sweeps are shown at the beginning of the recording (upper panel) and after 25 min (lower panel). Right: summary graphs ($n = 6$ experiments) show that prolonged recording conditions do not affect synaptic impact of either inward (upper inset) or outward currents (lower inset). *D*, spontaneous events recorded in distinct cell samples recorded with control intracellular solution (left, upper inset, $n = 15$ experiments) *versus* carbenoxolone-loaded pipettes (left, lower inset, $n = 12$ experiments, 100 μM). Right: summary plot showing that inclusion of carbenoxolone in the recording electrode selectively reduces outward currents.

potential unspecific effects in the rest of the network. We compared the synaptic impact of inward and outward currents in two populations of cells recorded with standard electrodes *versus* carbenoxolone-containing pipettes (100 μM, Fig. 6*D*). Synaptic impact of inward currents was 46.9 ± 7.0 pA s^{-1} ($n = 15$) in cells recorded with standard pipettes *versus* 37.5 ± 7.6 pA s^{-1} ($n = 12$) in neurons recorded with carbenoxolone-loaded electrodes ($P > 0.2$, M–W-test). In contrast, synaptic impact of outward currents was 3.1 ± 1.0 pA s^{-1} ($n = 15$) in cells recorded with control electrodes, but smaller ($P < 0.05$, M–W-test) in neurons recorded with drug included in the electrodes (0.9 ± 0.5 pA s^{-1}, $n = 12$). In conclusion, our voltage-clamp experiments show for the first time that, under the appropriate experimental conditions, propagated spontaneous synaptic currents can be identified in single-cell recordings.

Propagation of postsynaptic potentials in electrically coupled neurons

Next, we addressed the question of gap junction-mediated propagation of synaptic events in pairs of electrically coupled interneurons. After blockade of glutamatergic and $GABA_B$ receptor-mediated synaptic transmission, we took advantage of experimental conditions that allowed us to distinguish direct synaptic input from events propagated via gap junctions (Fig. 7*A*–*C*). The first cell of the pair (cell 1) was recorded with a chloride-loaded electrode (estimated $E_{GABA} = 0$ mV, see Methods for details), whereas a low-chloride pipette was used for the second neuron (cell 2, estimated $E_{GABA} = -80$ mV). Both cells were held at ~ -70 mV. Under these conditions, large spontaneous *depolarizing* events were expected in cell 1 because of the large driving force (i.e. $V_m - E_{GABA} = -70$ mV). In contrast, the driving force in cell 2 was expected to be smaller and of opposite direction (+10 mV), hence the observation of low-amplitude *hyperpolarizing* activity was predicted. In order to study whether events from cell 1 could propagate to cell 2, we used spontaneous events in cell 1 as a trigger to align the corresponding voltage recorded in cell 2. The degree of coupling of synaptic events between the two neurons (syn coupling coefficient) was 0.041 ± 0.006, which compared to 0.059 ± 0.008 for the DC coupling coefficient (Fig. 7*D*). Thus, paired recordings from electrically coupled

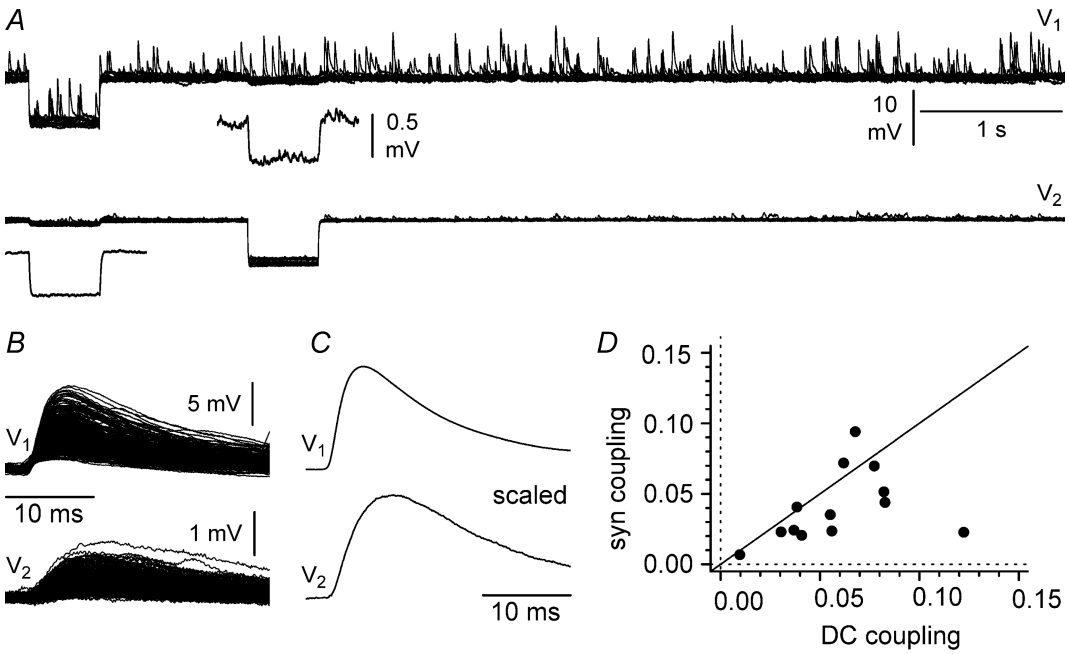

Figure 7. Propagation of postsynaptic events in pairs of electrically coupled interneurons held at −70 mV in current-clamp configuration
A, simultaneous recordings from cell 1 (V_1, high-chloride electrode, estimated $E_{GABA} = 0$ mV) and cell 2 (V_2, low-chloride electrode, estimated $E_{GABA} = -80$ mV). Notice the presence of large-amplitude depolarizing events in cell 1, and of much smaller amplitude in cell 2. Several ($n = 14$) sweeps are superimposed. At the beginning of every sweep, a current step (−100 pA amplitude, 500 ms duration) was sequentially injected in the two neurons to verify electrical coupling. Insets show averaged traces at a magnified scale. *B*, simultaneous depolarizing activity in the two cells is revealed by using postsynaptic potentials in cell 1 as a trigger to align activity in cell 2. Notice the presence of depolarizing synchronous events in cell 2, despite being held above the estimated E_{GABA}. A total of 284 sweeps are superimposed. *C*, scaled average in both neurons: notice the slower kinetics of the activity in cell 2. *D*, summary plot relating steady state (DC coupling) to synaptic propagation (syn coupling). The identity line is shown for reference.

interneurons apparently suggested that postsynaptic events can propagate from one neuron to another via gap junctions. Furthermore, we decided to compare propagation of the events in control conditions *versus* in the presence of the gap junction uncoupler carbenoxolone. As shown in Fig. 8*A–C*, we verified that external application of carbenoxolone (100 or 500 μM to speed up its blockade) reduced steady-state coupling. DC coupling decreased from 0.056 ± 0.010 to 0.001 ± 0.000 in the presence of the drug ($n = 10$, $P < 0.05$, W-test), and reduced the junctional conductance. The effective junctional conductance in control conditions was estimated to be 422.1 ± 58.7 pS ($n = 13$) compared to 16.8 ± 6.6 pS ($n = 10$) in the presence of the drug ($P < 0.05$, M–W-test). After having verified that carbenoxolone was effective in reducing electrical coupling, we observed that propagation of synaptic events was severely depressed (Fig. 8*D* and *F*), indicating that the synchronous activity observed in cell 2 was due to spread of postsynaptic potentials via gap junctions. The synaptic coupling coefficient decreased from 0.042 ± 0.006 in control conditions to 0.008 ± 0.004 in the presence of carbenoxolone (Fig. 8*F*, $n = 10$, $P < 0.05$, W-test). As a further control, we also verified that no propagated activity was detected in pairs of cells that were not electrically coupled. In 19 paired recordings from uncoupled neurons, no propagation was observed (Fig. 8*E*).

Properties of GABAergic input to stratum lacunosum moleculare interneurons during 4-aminopyridine-induced network activity

Next, we decided to study the significance of the propagation of synaptic input in stratum lacunosum moleculare interneuron networks during GABAergic input-driven activity in the absence of ionotropic glutamatergic transmission (Perreault & Avoli, 1989, 1992; Lamsa & Kaila, 1997; Perkins, 2002). In the presence of glutamatergic ionotropic and $GABA_B$ receptor antagonists, voltage-clamp recordings from stratum lacunosum moleculare interneurons in slices exposed to 4-aminopyridine (50–100 μM) revealed the spontaneous occurrence of large (amplitude at -65 mV was -3.8 ± 0.8 nA when high-chloride intracellular solution was used, $n = 5$ cells) and long-lasting (half-width at -65 mV was 843 ± 103 ms, $n = 5$ cells) events, which were strongly depressed by gabazine (Fig. 9*A* and *B*). We will refer to these currents as giant postsynaptic currents (giant PSCs). Linear fitting of the experimental current–voltage relationship of giant PSCs obtained from five cells recorded with high-chloride intracellular solution (identical to the one used for the recordings of Fig. 2) yielded a conductance of 61.5 nS (which compared to 1.6 nS for the *largest* spontaneous events recorded in quiescent slices, as shown in Fig. 2). Thus, a rather conservative estimate indicates that at the peak of 4-aminopyridine-induced network activity, synchronized GABAergic input is ~40 times larger than the largest

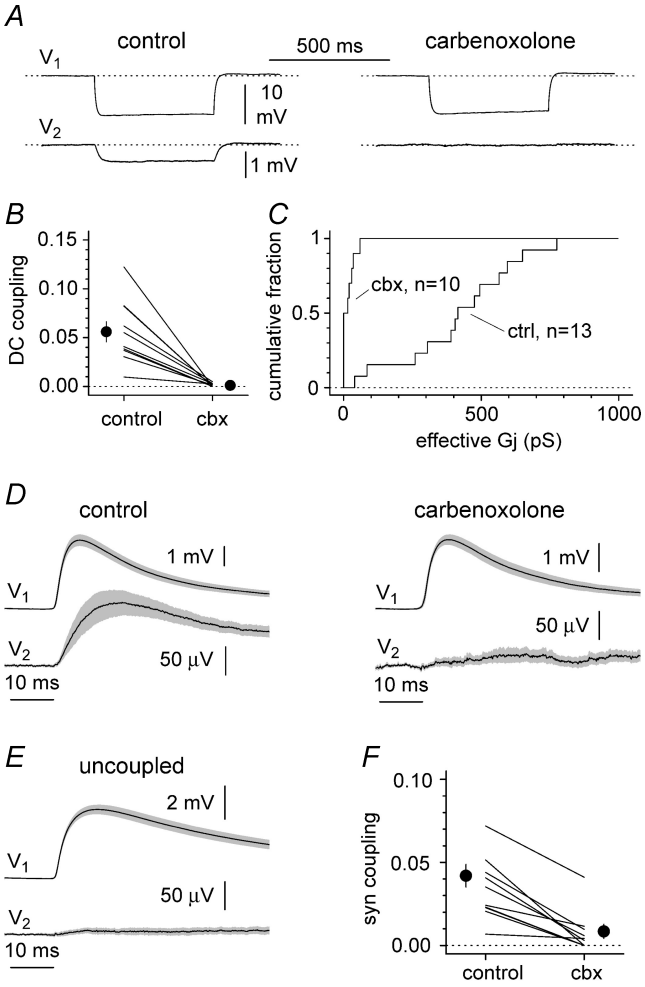

Figure 8. Pharmacological blockade of gap junction-propagated electrotonic pulses and synaptic potentials
A, recordings from an electrically coupled pair in control conditions (left) and in the presence of 500 μM carbenoxolone (right). A negative current pulse (-100 pA amplitude, 500 ms duration) was injected selectively in the first cell. Cell 1 (V_1) was recorded with a high-chloride electrode (estimated $E_{GABA} = 0$ mV), whereas a low-chloride pipette was used for cell 2 (V_2, estimated $E_{GABA} = -80$ mV). *B*, summary plots showing the effect of carbenoxolone (cbx) on the DC coupling. Notice the dramatic decrease of coupling in the presence of the drug. *C*, carbenoxolone-mediated blockade of the estimated effective junctional conductance (G_j). The summary graph shows the cumulative distributions of the G_j in control conditions (ctrl, $n = 13$ recordings) and in the presence of the drug (cbx 100 or 500 μM, $n = 10$ recordings) superimposed for comparison. *D*, left: average ± S.E.M. (grey area) of the mean synaptic events recorded from the same pairs analysed in *B*. Right: carbenoxolone abolishes the propagated events in the coupled cell. *E*, no propagation of synaptic events can be observed in electrically uncoupled pairs ($n = 19$ pairs). *F*, summary graph comparing synaptic coupling in connected pairs in control and in the presence of carbenoxolone. Notice the clear reduction of the synaptic coupling ($n = 10$ pairs).

putative unitary input. The reversal potential estimated from the fitting was −3 mV, in reasonable agreement with a predicted value of 0 mV. When we repeated the same experiment using low-chloride pipettes, biphasic currents were recorded close to the reversal potential, similarly to what described in pyramidal neurons (Perkins & Wong, 1996). The estimated reversal potential from five recordings was −35 mV (peaks of biphasic waveforms were averaged), which was largely different from the predicted value of −66 mV (Fig. 9*C*). Both components of the biphasic currents were strongly reduced by gabazine, as shown in Fig. 9*D*, $n = 5$ cells).

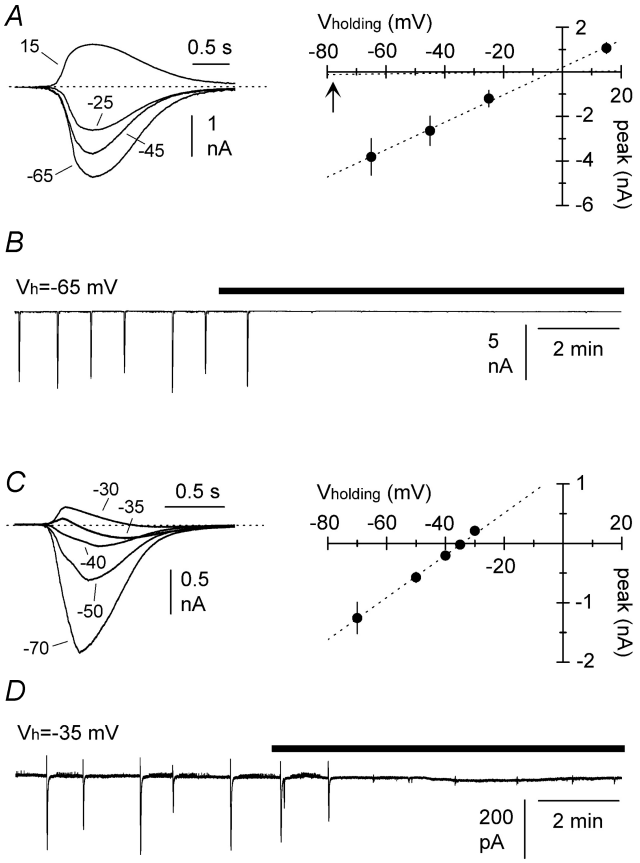

Figure 9. Current–voltage relationships of spontaneous giant GABAergic PSCs recorded in slices exposed to 4-aminopyridine (50–100 μM) in the absence of ionotropic glutamatergic transmission

A, *I–V* relationship obtained with high-chloride electrodes (identical intracellular solution to the one used in Fig. 2, see Methods for details). Left: superimposed averaged traces at different holding potentials (mV), as indicated. Right: summary plot from five experiments. Notice that the reversal potential is very close to the predicted value of 0 mV. The experimental points were fitted by linear regression (dotted line, $y = 0.06151x + 0.1953$, $r^2 = 0.998$, $P < 0.05$). The linear fit of the *I–V* relationship for spontaneous events obtained in slices not exposed to 4-aminopyridine (Fig. 2) is shown by the dotted line for comparison (arrow). Notice the large difference in the slope of the lines, reflecting the different conductances of the events. *B*, rapid blockade of spontaneous giant PSC recorded with high-chloride solutions following external gabazine application (black bar). Similar results were obtained in a total of five cells. Holding potential was −65 mV. *C*, *I–V* relationship of giant GABAergic PSCs recorded with low-chloride electrodes (see Methods for details). Left: averaged traces at various holding potentials, as indicated (mV). Notice that close to the reversal potential the waveform becomes biphasic. Right: summary graph from five experiments. The estimated reversal potential following the linear fit of the data ($y = 0.03553x + 1.221$, $r^2 = 0.998$, $P < 0.05$) is more depolarized than the predicted value (−35 mV *versus* −66 mV, respectively). *D*, both components of the biphasic waveform recorded at depolarized holding potentials ($V_h = -35$ mV) are sensitive to gabazine application (black bar). Similar results were observed in a total of five interneurons.

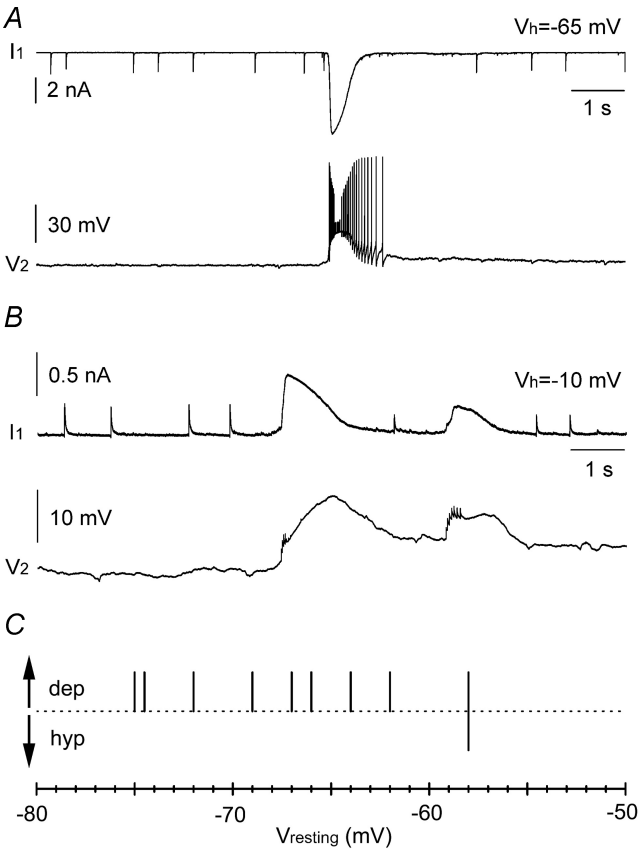

Figure 10. Giant PSCs are associated with excitation of stratum lacunosum moleculare interneurons

A, simultaneous recording from two interneurons in whole-cell voltage- (cell 1, I_1) and current-clamp (cell 2, V_2) configurations. Notice the strong spontaneous burst occurring during network activation. Cell 1 was recorded with high-chloride voltage-clamp intracellular solution and held at −65 mV, whereas cell 2 was recorded with low-chloride current-clamp pipette solution and its resting membrane potential was ∼−67 mV. *B*, double recording from interneurons in whole-cell voltage clamp (cell 1, I_1) and cell-attached current clamp $I = 0$ configuration (cell 2, V_2). Cell 1 was held at −10 mV, and was recorded with low-chloride voltage-clamp intracellular solution, whereas standard ACSF was used to fill the cell-attached pipette used to record from cell 2. The resting potential of cell 2 was ∼−72 mV. Notice the heavily filtered depolarizing responses and spikes in cell 2 occurring simultaneously to the giant PSCs recorded from cell 1. *C*, summary plot for nine experiments using non-invasive cell-attached configuration as in *B*. The direction (depolarising = dep; hyperpolarizing = hyp) of the voltage response recorded in cell 2 associated with network input recorded from cell 1 is plotted against the resting membrane potential. Only in one case was a mixed hyperpolarizing–depolarizing response observed in a cell with a relatively depolarized membrane potential.

In order to confirm that giant GABAergic events were associated with excitation in interneurons, we performed simultaneous double recordings in whole-cell voltage- and current-clamp configurations. As shown in Fig. 10*A*, the occurrence of giant spontaneous events in the cell under voltage clamp was mirrored by strong bursting activity in the neuron recorded in current-clamp ($n = 5$ double recordings). Similar results were obtained using non-invasive techniques, which preserve intracellular chloride gradients (Morikawa *et al.* 2003). Coupling whole-cell recording from one neuron to cell-attached current-clamp recording in the second cell of the pair confirmed the results obtained with double whole-cell recordings (Fig. 10*B*). The average resting membrane potential recorded in cell-attached configuration was -67.5 ± 1.9 mV ($n = 9$). In eight out of nine double recordings, giant PSCs recorded in the cell under voltage clamp were associated with depolarizing responses in the cell recorded in cell-attached configuration, whereas in one cell a biphasic hyperpolarizing–depolarizing response was observed (Fig. 10*C*).

Finally, we directly tested the propagation of excitatory GABAergic potential pharmacologically. As shown in Fig. 11*A*, application of carbenoxolone for 25 min drastically reduced the amplitude of network-driven giant PSCs (amplitude decreased from 1.4 ± 0.3 nA during the initial 5 min in control to 0.5 ± 0.1 nA in the last 5 min in the presence of the drug, $n = 8$ recordings, W-test, $P < 0.05$). As a control experiment, we verified that the decrease in network activity was not the result of unspecific run-down of the slice, by monitoring the amplitude of giant events for 30 min without drug application (amplitude was 638 ± 162 pA during the initial 5 min compared to 593 ± 146 pA during the last 5 min of the recording, $n = 6$ recordings, W-test, $P > 0.2$, Fig. 11*B*).

Discussion

This work reveals that GABAergic synaptic events can propagate via gap junctions across electrically coupled stratum lacunosum moleculare interneurons. Furthermore, propagated activity can be distinguished from direct postsynaptic events by electrophysiological means in voltage-clamp and current-clamp configurations. Our interpretation is based on electrophysiological and pharmacological data obtained from single and paired recordings, and is consistent with computational modelling results. We also show that the generation of giant PSCs recorded from stratum lacunosum moleculare interneurons is modulated by electrical coupling.

Mixed polysynaptic pathways

Despite its importance and indication from previous studies in invertebrate and non-cortical systems that this may be the case (for example, Decima, 1969; Martin & Pilar, 1963; Zipser & Bennett, 1976; Marder & Eisen, 1984; Slesinger & Bell, 1985; Pereda *et al.* 1995; Garcia-Perez *et al.* 2004; for a review of electrical coupling in the mammalian brain see Connors & Long, 2004; for a general review including older work see Bennett, 1977), the propagation of synaptic signals across gap junctions has yet not been studied in pairs of mammalian cortical neurons, and work has concentrated only on the transmission of spikes or steady-state electrotonic signals. The efficiency of propagation of synaptic potentials in cortical neurons has not been measured directly, and

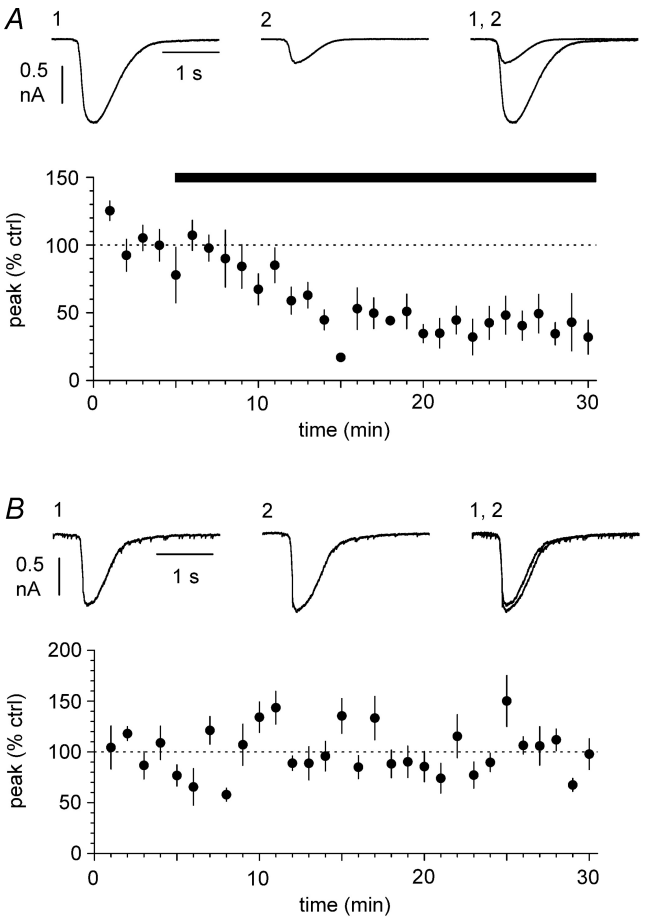

Figure 11. Gap junction blockade depresses giant PSCs recorded in stratum lacunosum moleculare interneurons
A, application of carbenoxolone (100 μM, black bar) strongly depresses the network-driven giant PSC recorded from slices exposed to 4-aminopyridine. Blockers of ionotropic glutamatergic synaptic transmission were present throughout. Data are from eight recordings. Holding potential was −60 mV. Insets show average traces in control conditions (1); in the presence of the drug (2); and superimposed (1, 2). *B*, similar plot to *A*, obtained from six interneurons not exposed to carbenoxolone. Note that network activity is maintained stable for the duration of the recording. Hence the effect of carbenoxolone shown in *A* cannot be attributed to time-dependent run-down of synchronization in the slice. Insets show averaged traces during the initial (1) and final (2) part of the recording, and superimposed (1, 2).

quantification is still lacking. It is important to underscore that the spreading of synaptic events differs from the more commonly studied propagation of artificially generated electrotonic signals or spikes, for at least three reasons. First, gap junction-mediated propagation of electrical signals is influenced by the kinetics of the signal itself (Galarreta & Hestrin, 1999; Price *et al.* 2005). Therefore, synaptic signals are likely to propagate less efficiently than steady-state voltages, but more efficiently than spikes. Second, the study of synaptic events offers insights on the propagation of electrical signals generated on the entire somatodendritic structure of the neuron, in contrast to artificial signals generated by strictly somatic current injections. Third, artificial electrotonic pulses are not associated with any change in membrane conductance, whereas synaptic events require the opening of synaptic channels and may affect dendritic voltage-dependent conductances.

Our results show that part of the spontaneous synaptic events recorded from a single hippocampal interneuron is the result of neurotransmitter release occurring on another cell. This type of polysynaptic transmission could be generated by the sequential chain of a chemical input that is directly targeting a neuron electrically coupled to another cell (Fig. 12*A*). We propose to term this network arrangement mixed polysynaptic pathway, because of the cooperation between chemical and electrical synapses. Studies in the neocortex (Simon *et al.* 2005) and in the hippocampus (Fukuda & Kosaka, 2000) have already demonstrated the close proximity of chemical synapses and gap junctions on the membrane of interneurons, thus identifying the potential structural basis underlying mixed polysynaptic pathways.

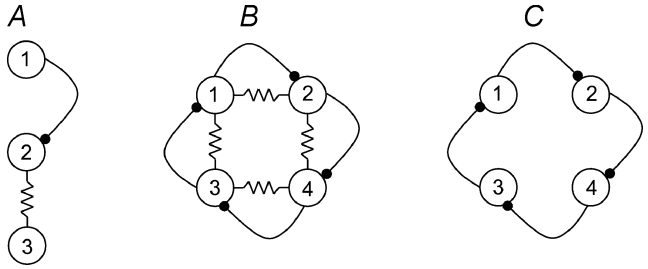

Figure 12. Simplified schematic cartoons illustrating the proposed pathway extension introduced by mixed polysynaptic pathways
A, direct neurotransmitter release from neuron 1 to neuron 2 can generate a postsynaptic potential in neuron 3, which is not directly innervated by neuron 1. *B*, during network synchronization, electrical coupling may serve as a recurrent circuit extending synaptic divergence. Notice, for example, that the chemical postsynaptic potential generated by neuron 1 onto neuron 2 can be propagated also to neuron 4 and back to neuron 1, despite the lack of direct chemical connectivity. Similar observations extend to the rest of the network. *C*, the same network in the absence of gap junctions. Propagation of postsynaptic potentials is strictly determined by the anatomical chemical connectivity. The experimental comparison of network synchronization in stratum lacunosum moleculare interneurons in scenarios reflected by *B versus C* is addressed experimentally in Fig. 11.

Dissociation of direct and propagated activity: technical considerations

Our experiments have taken advantage of the biophysical properties of the $GABA_A$ receptor, which is mostly permeable to chloride ions (Bormann *et al.* 1987), and of the whole-cell variation of the patch-clamp techniques, which allows the manipulation of the ionic conditions of the recorded neurons. It is important to emphasize that chloride manipulation was essential to allow the unambiguous dissociation of direct *versus* propagated input. Indeed, the identification of propagated events was strengthened by the *simultaneous* requirements of: (i) a polarity incompatible with the one predicted for synaptic events generated by direct neurotransmitter release; and (ii) pharmacological sensitivity to the gap junction uncoupler carbenoxolone. Although the specificity of carbenoxolone for gap junctions is still controversial (for work reporting: (i) lack of gap junction-unrelated effects onto the excitability of pyramidal cells in hippocampal slices see Kohling *et al.* 2001; Margineanu & Klitgaard, 2001; Schmitz *et al.* 2001; (ii) lack of direct effects on membrane properties and excitability of hippocampal interneurons see Yang & Michelson, 2001; (iii) increased excitability of pyramidal cells in hippocampal slices see Jahromi *et al.* 2002; (iv) depression of excitability of pyramidal cells in hippocampal cultures see Rouach *et al.* 2004), we believe that unspecific effects on neuronal membrane excitability, if present at all, should not significantly affect the interpretation of our results for the following reasons. First, carbenoxolone does not change the synaptic impact of GABAergic inward currents recorded at depolarized potentials, whereas it strongly depresses outward currents. Indeed, although bath application of carbenoxolone slightly increased the synaptic impact of inward currents, this increase was not statistically significant. If carbenoxolone depressed the excitability of the GABAergic network under study, this should be reflected by a decrease in the synaptic impact of all the spontaneous events recorded (both inward and outward), in contrast with our observation. Second, if carbenoxolone affected the intrinsic properties of the GABAergic network under study, external application to the entire slice would be expected to have largely different effects compared to a more limited exposure such as intracellular loading via a recording pipette containing QX-314. In contrast, our experimental results show similar results (no effect on synaptic impact of inward current, strong depression of synaptic impact of outward currents). Third, the time course of the effect of carbenoxolone on outward

currents is very similar to the one reported by Zsiros & Maccaferri (2005), which was associated with the direct demonstration of blockade of electrical coupling in paired recordings.

Propagated GABAergic input to the stratum lacunosum moleculare in quiescent and 4-aminopyridine-exposed slices

In order to boost the signal-to-noise ratio and to unambiguously distinguish propagated from direct input, our observations were made under elevated intracellular chloride conditions, and at depolarized potentials in voltage-clamp experiments, which may overestimate the importance of propagated input in a quiescent slice where E_{GABA} is potentially close to resting potentials. We did not directly address this point because of the promiscuity of electrical coupling in the stratum lacunosum moleculare network (Zsiros & Maccaferri, 2005), which would require measurements of E_{GABA} for every different subtype of interneuron participating in the network. Nevertheless, the observation of outward currents places limit to E_{GABA} in a subpopulation of coupled neurons, suggesting that, at least in a fraction of the coupled cells, E_{GABA} is likely to be close to resting potentials (estimated reversal for outward currents was -70 mV). In conclusion, the significance of propagated events in quiescent slices appears to be somewhat modest, as indicated by the fact that the synaptic impact of outward events recorded under favourable conditions was much smaller than the one of inward currents. However, three main considerations need to be highlighted. First, we evaluated gap junction-mediated propagation of synaptic events by *somatic* recordings, therefore potentially underestimating propagation to domains directly adjacent to *dendritic* gap junctions (Simon *et al.* 2005). Therefore, the degree of attenuation that we observed at the soma may not reflect propagated potentials at the dendrites, which could still play a significant role in the integration of local signals (Polsky *et al.* 2004). Technical limitations prevent a direct exploration of this issue: paired recording from membrane domains directly adjacent to the unknown site of the gap junction(s) would be required. Second, E_{GABA} is a dynamic variable, which can be modulated by the state of the network (Thompson & Gahwiler, 1989; Lamsa & Taira, 2003; but see also Perkins, 1999). Our experimental determination of the reversal potential for giant PSCs during dynamic network states suggests that synchronized giant GABAergic input onto stratum lacunosum moleculare interneurons is clearly excitatory. This interpretation was further strengthened by the converging results obtained with whole-cell and non-invasive cell-attached recordings, showing the synchronous occurrence of bursting/depolarizing responses and giant PSCs in the interneuronal network. These results explain very well the finding of Perkins (2002) that exogenous GABA puffed onto the stratum lacunosum moleculare activates an interneuron network. Third, although no quantitative work is available for interneurons located in the stratum lacunosum-moleculare of the hippocampus, studies in the neocortex suggest that individual interneurons may be electrically coupled to at least cells (Amitai *et al.* 2002; Fukuda *et al.* 2006). Therefore, the summation of depolarizing propagated events from many cells during synchronous activity could further enhance their impact on the target neuron.

We have directly addressed this point in a model of network synchronization that depends predominantly on $GABA_A$ receptor-mediated synaptic transmission. It is important to note that blockade of gap junctions under these dynamic conditions would be expected to eliminate an electrical coupling-based recurrent pathway spreading excitation (Fig. 12*B* and *C*). Indeed, our results show that synchronized giant PSCs recorded from stratum lacunosum moleculare interneurons are critically regulated by electrical coupling. Thus, it is important to underscore that our 'quiescent slice' approach was essential for the precise quantification and study of the biophysical properties underlying propagation of synaptic potentials, but that the significance of this mechanism may be especially related to dynamic network states. For example, a similar this type of network synchronization has been suggested to trigger the initiation of seizures in patients affected by Taylor's-type focal cortical dysplasia (Taylor *et al.* 1971; Avoli, 1996; D'Antuono *et al.* 2004). Furthermore, GABAergic mediated network hyperexcitability could spread across brain regions affected by loss of principal neurons, and with disrupted excitatory synaptic input such as mesial limbic structures of temporal lobe epilepsy patients with Ammon's horn sclerosis (Gloor, 1991). Intriguingly, 4-amynopiridine-induced experimental seizures *in vivo* have been reported to increase the expression of messenger RNA for various types of connexins in primary epileptic foci (Gajda *et al.* 2003), suggesting the possibility that positive feedback between epileptiform activity and the strength of electrical coupling might contribute to maintaining epileptic conditions. However, this effect was described *in vivo* after at least one hour of epileptic activity (Gajda *et al.* 2003), whereas our *in vitro* baseline exposure to 4-aminopyridine was much more limited before application of carbenoxolone. This suggests that this mechanism is unlikely to have played a major role under our experimental conditions.

Conclusions

In summary, we have studied the integration of synaptic potentials and electrical coupling in stratum lacunosum moleculare interneurons of the hippocampus. The

unambiguous identification of chemically mediated *versus* electrically propagated events has allowed us to give a quantitative estimate of the synaptic coupling in pairs of neurons. This mechanism is likely to play an important role in normal synchronized states of the network, and may contribute to epileptic seizures.

References

Abbott LF, Varela JA, Sen K & Nelson S (1997). Synaptic depression and cortical gain control. *Science* **275**, 220–224.

Amitai Y, Gibson JR, Beierlein M, Patrick S, Ho AM, Connors BW & Golomb D (2002). The spatial dimensions of electrically coupled networks of interneurons in the neocortex. *J Neurosci* **22**, 4142–4152.

Aradi I & Holmes WR (1999). Role of multiple calcium and calcium-dependent conductances in regulation of hippocampal dentate granule cell excitability. *J Comput Neurosci* **6**, 215–235.

Aradi I & Maccaferri G (2004). Cell type-specific synaptic dynamics of synchronized bursting in the juvenile CA3 rat hippocampus. *J Neurosci* **24**, 9681–9692.

Avoli M (1996). GABA-mediated synchronous potentials and seizure generation. *Epilepsy* **37**, 1035–1042.

Bartos M, Vida I, Frotscher M, Geiger JR & Jonas P (2001). Rapid signaling at inhibitory synapses in a dentate gyrus interneuron network. *J Neurosci* **21**, 2687–2698.

Bartos M, Vida I, Frotscher M, Meyer A, Monyer H, Geiger JR & Jonas P (2002). Fast synaptic inhibition promotes synchronized gamma oscillations in hippocampal interneuron networks. *Proc Natl Acad Sci U S A* **99**, 13222–13227.

Beblo DA & Veenstra RD (1997). Monovalent cation permeation through the connexin40 gap junction channels. Cs, Rb, K, Na, Li, TEA, TMA, TBA, and effects of anions Br, Cl, F acetate, aspartate, glutamate, and NO_3. *J Gen Physiol* **109**, 509–522.

Bennett MVL (1977). Electrical transmission: a functional analysis and comparison to chemical transmission. In *Handbook of Physiology*, section 1, *The Nervous System*, vol. I, *Cellular Biology of Neurons*, ed. Kandel E, pp. 357–416. American Physiological Society, Bethesda, MD.

Bennett MVL & Zukin SR (2004). Electrical coupling and neuronal synchronization in the mammalian brain. *Neuron* **41**, 495–511.

Bormann JH, Hamill OP & Sakmann B (1987). Mechanism of anion permeation through channels gated by glycine and gamma-aminobutyric acid in mouse cultured spinal neurones. *J Physiol* **385**, 243–286.

Connors BW & Long MA (2004). Electrical synapses in the mammalian brain. *Annu Rev Neurosci* **27**, 393–418.

D'Antuono M, Louvel J, Kohling R, Mattia D, Bernasconi A, Olivier A, Turak B, Devaux A, Pumain R & Avoli M (2004). $GABA_A$ receptor-dependent synchronization leads to ictogenesis in the human dysplastic cortex. *Brain* **127**, 1626–1640.

Deans MR, Gibson JR, Sellitto C, Connors BW & Paul DL (2001). Synchronous activity of inhibitory networks in neocortex requires electrical synapses containing connexin 36. *Neuron* **31**, 477–485.

Decima EE (1969). An effect of postsynaptic neurons upon presynaptic terminals. *Proc Natl Acad Sci U S A* **63**, 58–64.

Eskandari S, Zampighi GA, Leung DW, Wright EM & Loo DD (2002). Inhibition of gap junction hemichannels by chloride channel blockers. *J Membr Biol* **185**, 93–102.

Figl T, Lewis TM & Barry PH (2004). Liquid junction potential corrections. www.moleculardevices.com/pdfs/pCLAMP_AppNote_LJP_Corrections.pdf

Fricker D, Verheugen JA & Miles R (1999). Cell-attached measurements of the firing threshold of rat hippocampal neurones. *J Physiol* **517**, 791–804.

Fukuda T & Kosaka T (2000). Gap Junctions linking the dendritic network of GABAergic interneurons in the hippocampus. *J Neurosci* **20**, 1519–1528.

Fukuda T, Kosaka T, Singer W & Galuske RAW (2006). Gap junctions among dendrites of cortical GABAergic neurons establish a dense and widespread intercolumnar network. *J Neurosci* **26**, 3434–3443.

Gajda Z, Gyengesi E, Hermesz E, Ali SK & Szente M (2003). Involvement of gap junctions in the manifestation and control of the duration of seizures in rats in vivo. *Epilepsia* **44**, 1596–1600.

Galarreta M & Hestrin S (1998). Frequency-dependent synaptic depression and the balance of excitation and inhibition in the neocortex. *Nat Neurosci* **1**, 587–594.

Galarreta M & Hestrin S (1999). A network of fast-spiking cells in the neocortex connected by electrical synapses. *Nature* **402**, 72–75.

Garcia-Perez E, Vargas-Caballero M, Velazquez-Ulloa Minzoni A & De-Miguel FF (2004). Synaptic integration in electrically coupled neurons. *Biophys J* **86**, 646–655.

Gloor P (1991). Mesial temporal sclerosis: historical background and an overview from a modern prespective. In *Epilepsy Surgery*, ed. Luders H, pp. 689–703. Raven Press, New York.

Gulyas AI, Sik A, Payne JA, Kaila K & Freund TF (2001). The KCl cotransporter, KCC2, is highly expressed in the vicinity of excitatory synapses in the rat hippocampus. *Eur J Neurosci* **13**, 2205–2217.

Hestrin S & Galarreta M (2005). Electrical synapses define networks of neocortical GABAergic neurons. *Trends Neurosci* **28**, 304–309.

Hines ML & Carnevale NT (1997). The NEURON simulation environment. *Neuronal Comput* **9**, 1179–1209.

Hormuzdi SG, Pais I, LeBeau F, Towers SK, Rozov A, Buhl EH, Whittington MA & Monyer H (2001). Impaired electrical signaling disrupts frequency oscillations in connexin 36-deficient mice. *Neuron* **31**, 487–495.

Jahromi SS, Wentland K, Piran S & Carlen PL (2002). Anticonvulsant actions of gap junctional blockers in an in vitro seizure model. *J Neurophysiol* **88**, 1893–1902.

Kohling R, Gladwell SJ, Bracci E, Vreugdenhil M & Jefferys JG (2001). Prolonged epileptiform bursting induced by 0 Mg^{2+} in rat hippocampal slices depends on gap junctional coupling. *Neuroscience* **105**, 579–587.

Kosaka T & Hama K (1985). Gap junctions between non-pyramidal cell dendrites in rat hippocampus (CA1 and CA3 regions): a combined Golgi-electron microscope study. *J Comp Neurol* **231**, 150–161.

Lamsa K & Kaila K (1997). Ionic mechanisms of spontaneous GABAergic events in rat hippocampal slices exposed to 4-aminopyridine. *J Neurophysiol* **78**, 2582–2591.

Lamsa K & Taira T (2003). Use-dependent shift from inhibitory to excitatory $GABA_A$ receptor action in SP–O interneurons in the rat hippocampal CA3 area. *J Neurophysiol* **90**, 1983–1995.

Marder E & Eisen JS (1984). Electrically coupled pacemaker neurons respond differently to same physiological inputs and neurotransmitters. *J Neurophysiol* **51**, 1362–1374.

Margineanu DG & Klitgaard H (2001). Can gap junction blockade preferentially inhibit neuronal hypersynchrony vs. excitability? *Neuropharmacology* **41**, 377–383.

Martin AR & Pilar G (1963). Dual mode of synaptic transmission in the avian ciliary ganglion. *J Physiol* **168**, 443–463.

Meyer AH, Katona I, Blatow M, Rozov A & Monyer H (2002). In vivo labeling of parvalbumin-positive interneurons and analysis of electrical coupling in identified neurons. *J Neurosci* **22**, 7055–7064.

Morikawa H, Khodakhah K & Williams JT (2003). Two intracellular pathways mediate glutamate receptor-induced Ca^{2+} mobilization in dopamine neurons. *J Neurosci* **23**, 149–157.

Neher E (1992). Correction for liquid junction potentials in patch clamp experiments. *Meth Enzymol* **207**, 123–131.

Pereda AE, Bell TD & Faber DS (1995). Retrograde synaptic communication via gap junctions coupling auditory afferents to the Mauthner cell. *J Neurosci* **15**, 5943–5955.

Perkins KL (1999). Cl- accumulation does not account for the depolarizing phase of the synaptic GABA response in hippocampal pyramidal cells. *J Neurophysiol* **82**, 768–777.

Perkins KL (2002). GABA application to hippocampal CA3 or CA1 stratum lacunosum-moleculare excites and interneuron network. *J Neurophysiol* **87**, 1404–1414.

Perkins KL & Wong RK (1996). Ionic basis of the postsynaptic depolarizing GABA response in hippocampal pyramidal cells. *J Neurophysiol* **76**, 3886–3894.

Perreault P & Avoli M (1989). Effects of low concentration sof 4-aminopyridine on CA1 pyramidal cells of the hippocampus. *J Neurophysiol* **61**, 953–970.

Perreault P & Avoli M (1992). 4-aminopyridine-induced epileptiform activity and a GABA-mediated long-lasting depolarization in the rat hippocampus. *J Neurosci* **12**, 104–115.

Polsky A, Mel BW & Schiller J (2004). Computational subunits in thin dendrites of pyramidal cells. *Nat Neurosci* **7**, 567–569.

Price CJ, Cauli B, Kovacs ER, Kulik A, Lambolez B, Shigemoto R & Capogna M (2005). Neurogliaform neurons form a novel inhibitory network in the hippocampal CA1 area. *J Neurosci* **25**, 6775–6786.

Rouach N, Segal M, Koulakoff A, Giaume C & Avignone C (2004). Carbenoxolone blockade of neuronal activity in culture is not mediated by an action on gap junctions. *J Physiol* **553**, 729–745.

Schmitz D, Schuchmann S, Fisahn A, Draguhn A, Buhl EH, Petrasch-Parwez E, Dermietzel R, Heinemann U & Traub RD (2001). Axo-axonal coupling, a novel mechanism for ultrafast neuronal communication. *Neuron* **31**, 831–849.

Simon A, Szabolcs O, Molnar G, Szabadics J & Tamas G (2005). Gap junctional coupling between neurogliaform cells and various interneuron types in the neocortex. *J Neurosci* **25**, 6278–6285.

Slesinger P & Bell CC (1985). Primary afferent fibers conduct impulses in both directions under physiological stimulus conditions. *J Comp Physiol* **157**, 15–22.

Srinivas M, Rozental R, Kojima T, Dermietzel R, Mehler M, Condorelli DF, Kessler JA & Spray DC (1999). Functional properties of channel formed by the neuronal gap junction protein connexin36. *J Neurosci* **19**, 9848–9855.

Stell BM & Mody I (2002). Receptor with different affinities mediated phasicand tonic GABA(A) conductances in hippocampal neurons. *J Neurosci* **22**, 1–5.

Szabadics J, Lorincz A & Tamas G (2001). Beta and gamma frequency synchronization by dendritic gabaergic synapses and gap junctions in a network of cortical interneurons. *J Neurosci* **21**, 5824–5831.

Taylor DC, Falconer MA, Bruton CJ & Corsellis JA (1971). Focal dysplasia of the cerebral cortex in epilepsy. *J Neurol Neurosurg Psychiatry* **34**, 369–387.

Teubner B, Degen J, Sohl G, Guldenagel M, Bukauskas FF, Trexler EB, Verselis VK, De Zeeuw CI, Lee CG, Kozak CA, Petrasch-Parwez E, Dermietzel R & Willecke K (2000). Functional expression of the murine connexion 36 gene coding for a neuron-specific gap junction protein. *J Membr Biol* **176**, 249–262.

Thompson SM & Gahwiler BH (1989). Activity dependent dishinibition. I. Repetitive stimulation reduces IPSP driving force and conductance in the hippocampus in vitro. *J Neurophysiol* **61**, 501–511.

Tsodyks MV & Markram H (1997). The neural code between neocortical pyramidal neurons depends on neurotransmitter release probability. *Proc Natl Acad Sci U S A* **94**, 719–723.

Venance L, Rozov A, Blatow M, Burnashev N, Feldmayer D & Monyer H (2000). Connexin expression in electrically coupled postnatal rat brain neurons. *Proc Natl Acad Sci U S A* **97**, 10260–10265.

Vida I, Bartos M & Jonas P (2006). Shunting inhibition improves robustness of gamma oscillations in hippocampal interneuron networks by homogeneizing firing rates. *Neuron* **49**, 107–117.

Yamada WM, Koch C & Adams PR (1989). Multiple channels and calcium dynamics. In *Methods in Neuronal Modeling: from Synapses to Networks*, ed. Koch C & Segev I, pp. 97–134. MIT Press, Cambridge, MA.

Yang Q & Michelson H (2001). Gap junctions synchronize the firing of inhibitory interneurons in guinea pig hippocampus. *Brain Res* **907**, 139–143.

Zhang XL, Zhang L & Carlen PL (2004). Electrotonic coupling between stratum oriens interneurones in the intact in vitro mouse juvenile hippocampus. *J Physiol* **558**, 825–839.

Zipser B & Bennett MVL (1976). Responses of cells of posterior lateral line lobe to activation of electroreceptors in a Mormyrid fish. *J Neurophysiol* **39**, 712.

Zsiros V & Maccaferri G (2005). Electrical coupling between interneurons with different excitable properties in stratum lacunosum-moleculare of the juvenile CA1 rat hippocampus. *J Neurosci* **25**, 8686–8695.

Acknowledgements

We would like to thank Dr J. Singer for critically reading the manuscript, Dr M. Martina for comments on a previous version of the work, Dr J. Dempster (University of Strathclyde) for providing us with the WCP analysis package, and Mrs M. Maccaferri for editorial assistance. This work was supported by National Institute of Mental Health Grant MH067561 (G.M).

Supplemental material

The online version of this paper can be accessed at:
DOI: 10.1113/jphysiol.2006.123463
http://jp.physoc.org/cgi/content/full/jphysiol.2006.123463/DC1
and contains supplemental material consisting of a figure.

This material can also be found as part of the full-text HTML version available from http://www.blackwell-synergy.com